JOURNAL OF APPLIED ELECTROCHEMISTRY 25 (1995) 556–564

Influence of Ge^{4+} and Pb^{2+} ions on the kinetics of zinc electrodeposition in acidic sulphate electrolyte

R. ICHINO, C. CACHET, R. WIART*

UPR15 du CNRS, Physique des Liquides et Electrochimie, Université Pierre et Marie Curie, Tour 22, 4 place Jussieu, 75252 Paris Cedex 05, France

Received 26 July 1994; revised 18 October 1994

The effect of Ge^{4+} ions, a deleterious impurity for zinc deposition in acidic sulfate electrolytes, and that of Pb^{2+} ions, which inhibit hydrogen evolution, have been investigated by means of steady-state polarization curves and impedance analysis. Typical impedance plots have been shown to characterize the processes of zinc deposition, hydrogen evolution on zinc, and hydrogen evolution on adsorbed germanium. From changes in the double layer capacitance, the charge transfer resistance and the low-frequency relaxation processes, it is concluded that lead adsorbed on zinc generates a lessened activation of hydrogen evolution with increasing cathodic potential, and enhances the formation of H_{ad} on the zinc deposit. With the addition of Pb^{2+} ions to the Ge^{4+}-containing electrolyte, the features characteristic of zinc deposition are observed to prevail in the electrode impedance.

1. Introduction

As the electrochemical base of zinc winning is that the overpotential of hydrogen evolution on zinc is very high in comparison with any other metals, removing some impurities from electrolyte and the effects of impurities on zinc electrowinning are important matters in the electrolysis process. The impurities behave as follows: when the impurity is a more noble metal than zinc, it can deposit easily and decreases the purity of the zinc. Moreover, when the overpotential of hydrogen evolution on the deposited impurity is low, the impurity promotes hydrogen evolution and leads to a decrease in current efficiency. The impurities often induce the redissolution of zinc deposits, change the morphology of deposits, and this behaviour affects the operation cost.

Zinc deposition is affected by bath acidity, temperature, current density, the nature and concentration of impurities and substrates, and the effects have been reported mainly in terms of current efficiency, morphology, orientation and cyclic voltammetry [1–8]. Maja *et al.* [1] have shown that the deleterious effect of impurities on current efficiency of zinc deposition follows in the order: Ge > Sb > Ni > Co > Bi > Cu > As > Sn.

Zinc electrowinning in highly acidic sulphate electrolytes containing metal impurities sometimes shows an 'induction period' [4, 9–11]. Following this period, a characteristic spontaneous self-dissolution of zinc deposits occurs down to the aluminium substrate, with simultaneous hydrogen evolution. After complete dissolution, zinc deposition restarts on the aluminium substrate. The induction period is affected by the above mentioned factors on zinc deposition. On the other hand, a certain impurity such as lead is known to impede hydrogen evolution and prevent the current efficiency from decreasing [6, 7, 12].

Some organic additives such as glue, gum arabic and 2-butyn-1,4-diol, etc., are known to improve both the current efficiency and the quality of deposits, which are decreased by harmful impurities such as germanium, antimony and nickel [9, 13–18]. Germanium and antimony show significant interaction with glue and the amount of glue added into an electrolyte must be optimum to satisfy a good balance in the relative concentration of metal and organic impurities. Mackinnon *et al.* [15] demonstrated the effect of increasing germanium concentration on the current efficiency of zinc deposition from an electrolyte containing a certain amount of glue. They showed that there was a gradual decrease in current efficiency with increasing germanium concentration.

Consequently, to have some accurate information about the effects of impurities on zinc deposition, zinc dissolution and hydrogen evolution should contribute to the productivity and the quality control of zinc electrowinning. But there are few reports about the effect of impurities on the mechanism of zinc deposition. Reports [10, 11, 19, 20] on the effect of nickel on zinc deposition using electrochemical impedance analysis and simulations of reactions on cathode have been published. These showed that not only the impurity metal in the electrolyte, but also the oxidized species produced at the anode, characterize the zinc deposition behaviour.

In the present paper the effect of germanium, one of the harmful elements, which is known to increase hydrogen evolution and redissolution of zinc deposits during zinc deposition [4, 5, 14, 15], is investigated on

* Author to whom correspondence should be addressed.

0021-891X 1995 Chapman & Hall

the basis of steady-state polarization curves and impedance analysis. Also, the influence of lead is studied with a view to compensating for the deleterious effect of germanium. In order to obtain accurate information on these effects, all experiments were performed using an electrolysis cell with separate compartments so as to prevent the possible influence of anodically produced oxidized species on zinc deposition.

2. Experimental details

Experimental details have been described previously [11]. The electrolysis cell was thermostatted at 38° C. To separate the anode from the cathode, a Nafion® diaphragm (Dupont de Nemours) was used between a Teflon holder and a glass container. The volume of electrolyte contained within each separated compartment was about 0.15 dm^3. The cathode and reference electrodes were placed in the inner compartment which was used for zinc deposition. Two different cathodes, a pure aluminium (99.999% purity, Johnson–Matthey, specpure) and a pure zinc (same as aluminium), were used, whose effective surfaces were vertical and parallel to the symmetry axis of the cell. Their surface area was 0.2 cm^2 obtained from a 0.5 cm diameter cylindrical metal, and they were insulated with epoxide resin (Buehler). Before electrolysis, the cathode surface was polished with emery paper (grit 1200). The reference electrode consisted of mercury/mercurous sulphate electrode in saturated potassium sulphate (SSE), used with two compartments separated by fritted glass. The counter electrode was a platinum gauze cylinder placed in the outer compartment of the cell.

The base electrolyte was made of 55 g dm^{-3} zinc from $ZnSO_4 \cdot 7H_2O$ and 120 g dm^{-3} H_2SO_4 with pure water, that was doubly ion-exchanged and twice distilled in a quartz apparatus. GeO_2 (Aldrich, 99.999%, Electronic grade) was dissolved in dilute HCl solution and a certain amount of this solution was added to the electrolyte so as to set the concentration of germanium 0.5 mg dm^{-3}. $Pb(NO_3)_2$ was dissolved in pure water and this solution was added to the electrolyte to give 10 mg dm^{-3} of lead. Except for GeO_2, all chemicals were Merck products of analytical grade purity and the maximum levels of impurities in the electrolyte were: Ca, K, Li, Mg, Na, Pb 2ppm; Cd, Cu, Fe, Sr 1 ppm; Mn 0.6 ppm; As 0.1 ppm.

Steady-state polarization curves and impedance measurements in the frequency range 60 kHz to 6 mHz were performed automatically using a frequency response analyser (Solartron SI 1250) and an electrochemical interface (Solartron SI 1286) controlled by a microcomputer (IBM PS/2 model 35slc) with software (FRACOM). Potentiostatic curves were obtained by potential steps of 10 mV from $U = -1.4$ V up to -1.5 V vs SSE, or from $U = -1.6$ V down to -1.4 V vs SSE, and waiting for current stabilization for 15 min at each potential U. The high frequency limit of electrode impedance yields the electrolyte resistance, R_e, which was used to correct the ohmic drop, $R_e i$, in the steady-state polarization curves i/E, with $|E| = |U| - R_e i$. This electrolyte resistance was measured at each potential and the values ranged between 0.32 and 0.83 $\Omega\,cm^2$, depending on the deposit growth or dissolution and on the presence of bubbles on the electrode surface.

Deposits for SEM observation were prepared under potentiostatic conditions by stepping down the potential from $U = -1.6$ V, and waiting for 50 min at each potential in order to agree with the conditions for impedance measurements.

3. Results and discussion

3.1. *Steady-state polarization curves and deposit morphology*

The steady-state polarization curves of zinc deposition on the aluminium cathode, recorded under potentiostatic conditions from $U = -1.6$ V to -1.4 V, are depicted in Fig. 1. Curve 1 was obtained in the base electrolyte, curve 2 in the presence of 0.5 mg dm^{-3} germanium, curve 3 in 10 mg dm^{-3} lead-containing electrolyte and curve 4 with both additives, respectively; all curves are corrected for ohmic drop. Curve 1 shows a plateau at the low cathodic potentials (from -1.45 to -1.48 V), and a branch corresponding to zinc deposition at more cathodic potentials. The current plateau (0.3 mA cm^{-2}) on the polarization curve results from the fact that the electrode seems to be blocked, as already reported [20], and the corrosion potential is

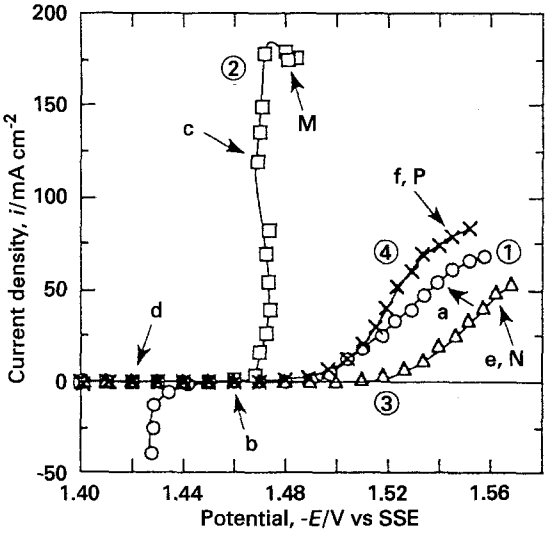

Fig. 1. Steady-state polarization curves i/E of zinc deposition obtained on aluminium electrode from $U = -1.6$ V down to -1.4 V vs SSE. Curve 1: base electrolyte; curve 2: with 0.5 mg dm^{-3} germanium; curve 3: with 10 mg dm^{-3} lead; curve 4: with both additives. Points a: $E = -1.539$ V on curve 1; b: $E = -1.46$ V on curve 1; c: $E = -1.469$ V on curve 2; d: $E = -1.42$ V on curve 2; e: $E = -1.562$ V on curve 3; f: $E = -1.545$ V on curve 4; M: $E = -1.48$ V on curve 2, N: the same as point e, P: the same as point f.

less noble (−1.44 V) than that (−1.41 V) obtained without a diaphragm [20].

On the other hand, in the case of curve 2, obtained with germanium, it is found that the current density first increases and then decreases abruptly with decreasing cathodic overpotential. The initial increase probably reflects the roughening of the zinc deposit before its dissolution and hydrogen evolution was observed on the cathode at all potentials. At potentials less cathodic than −1.46 V, the current density was about 0.01 mA cm^{-2} and corresponded to hydrogen evolution on the aluminium substrate as the dissolution of zinc was complete.

Instead of deposits covering the whole disc electrode generally obtained from the additive-free electrolyte, only a ring-shaped deposit was obtained from germanium-containing electrolyte. As exemplified in Fig. 2(a), the deposit had a definite ring shape at high cathodic potential. At lower potentials, it consisted of scattered grains on a ring-like locus, due to the dissolution of the ring-shaped deposits. The adhesion between zinc deposits and substrate in the latter case was very weak and the deposits were easily removed from the substrate. It appears that the corrosion and dissolution of the deposits with decreasing cathodic polarization, are directly connected to the vertical slope of the polarization curve 2 in Fig. 1.

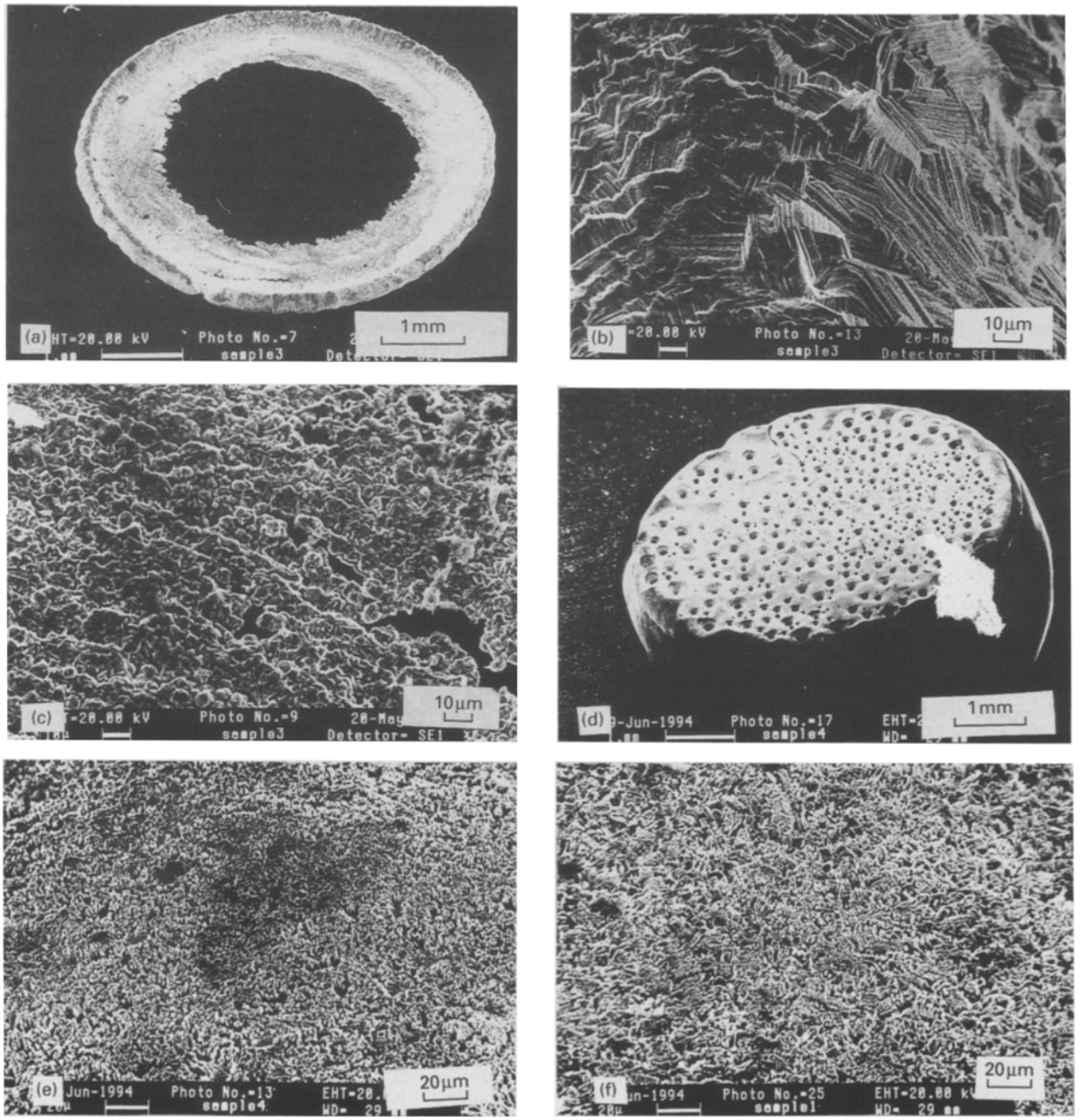

Fig. 2. SEM photographs of the surface of zinc deposits. (a) Overall feature of the deposit obtained from the germanium-containing electrolyte at point M in Fig. 1; (b) outer periphery part of the deposit in (a); (c) inner periphery part of the deposit in (a); (d) overall feature of the deposit obtained with both additives at point P in Fig. 1; (e) detail of (d); (f) obtained in the lead-containing electrolyte at point N in Fig. 1.

Figures 2(b) and 2(c) show the electrode morphology at the outer periphery and at the inner periphery, respectively, of a ring-deposit obtained at point M ($E = -1.48$ V) in Fig. 1. The presence of germanium in the electrolyte has no significant effect on the morphology of the non-dissolved region, Fig. 2(b), where the features are similar to those obtained from additive-free electrolyte. At the inner periphery, the grains were partially dissolved and the edge of each zinc crystal is roundish, Fig. 2(c).

Our results are very similar to those already reported in the literature. Mackinnon *et al.* [15] showed that the redissolution of zinc deposits started at the top-centre of square-shaped cathodes whose surface was set stationary and vertical, then gradually extended towards the sides and bottom of deposits, and that vigorous hydrogen evolution and zinc redissolution were observed to occur at cathodic potentials. Umetsu *et al.* [5] also reported the effect of germanium on zinc morphology and showed that the zinc deposits redissolved even under galvanostatic cathodic conditions. Therefore, the morphology of zinc deposits was observed to be changed from an accurate crystal form into a collapsed form and, finally, the remaining zinc deposits acquired complicated features as the concentration of germanium increased.

In comparison with the results obtained from the base electrolyte (curve 1 in Fig. 1), the current density obtained with the lead-containing electrolyte (curve 3) is strongly inhibited at cathodic and anodic potentials. This inhibition results from lead adsorbed or codeposited with zinc on the active sites where hydrogen evolution and zinc deposition occurred. In particular, it was reported that a dendritic deposition of zinc is inhibited by Pb^{2+} ions which adsorb or codeposit on active sites like the tops of dendrites [21–23]. Moreover, lead has a higher overpotential of hydrogen evolution than zinc, thus increasing the current efficiency of zinc deposition [6, 7, 12]. However, as lead also inhibits the zinc deposition reaction, the current density is lower than that without additive. When zinc deposition takes place at highly cathodic potentials, the inhibiting effect of Pb^{2+} ions is progressively weakened, because their low concentration causes their discharge to become diffusion-controlled. On the other hand, the codeposition of lead with zinc produces a lead-zinc alloy on the electrode surface [7, 24] whose dissolution is passivated; the current density between -1.41 V and -1.49 V is lower (about 0.07 mA cm^{-2}) than on curve 1, and the corrosion potential becomes noble.

The authors have shown previously that similar behaviour occurs in the cathodic domain produced by the presence of trace lead in acidic sulphate electrolyte [11]. The use of a rotating disc electrode increased the inhibition of the deposition process. The inhibition was shown to vanish, however, with increasing current density due to the deposition of trace lead under diffusion-controlled conditions [7, 11].

Curve 4 in Fig. 1 was obtained with both germanium and lead. It clearly appears that lead in the electrolyte nearly suppressed the effect of germanium on hydrogen evolution though a few bubbles remained on the electrode. The current density on the cathodic branch of curve 4 is slightly higher than that on curve 1 due, probably, to both a roughened deposit surface consequent on the competitive adsorption and codeposition of Pb^{2+} and Ge^{4+} ions, and the small contribution of the remaining hydrogen evolution on germanium sites.

With the presence of both additives, zinc deposits covering the whole disc electrode were obtained, Fig. 2(d). The presence of bubble traces is a feature of these deposits. A small grain size characterizes these deposits. Fig. 2(e), and the size reduction can be ascribed to the influence of lead in the electrolyte, which generates a similar deposit morphology when it is used alone as shown in Fig. 2(f).

It thus appears that the effect of lead on germanium is similar to that of organic additives in terms of improvement of current efficiency: lead behaves as an efficient inhibitor against hydrogen evolution originated by germanium.

As the existence of germanium stimulates the hydrogen evolution reaction, it is necessary to know the effect of germanium when only hydrogen evolution takes place on the cathode. A 120 g dm^{-3} H_2SO_4 solution was prepared for this purpose, that is, zinc ions were excluded from electrolyte, and a pure zinc metal and a pure aluminium metal were used as working electrodes.

Figure 3 shows the polarization curves for hydrogen evolution on zinc from $U = -1.6$ V down to -1.4 V. Curve 1 was obtained in the zinc-free sulfuric electrolyte without additive, curve 2 with germanium, curve 3 with lead and curve 4 with both germanium and lead, respectively. The hydrogen

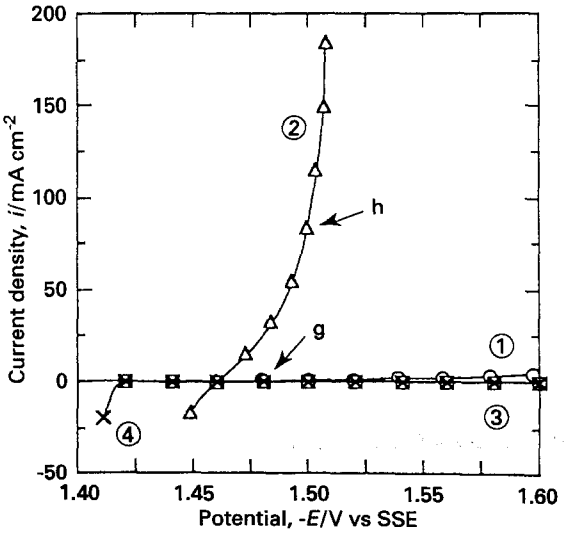

Fig. 3. Steady state polarization curves i/E of hydrogen evolution obtained on zinc electrode from $U = -1.6$ V down to -1.4 V vs SSE in the 120 g dm^{-3} H_2SO_4 solution. Curve 1: without additive; curve 2: with 0.5 mg dm^{-3} germanium; curve 3: with 10 mg dm^{-3} lead; curve 4: with both additives. Points g: $E = -1.48$ V on curve 1; h: $E = -1.5$ V on curve 2.

evolution reaction on curve 2 is less polarized and the current density is much higher than on the other curves. It appears that germanium facilitates the hydrogen evolution reaction on the zinc electrode.

On the other hand, the current density obtained in lead-containing electrolytes (curves 3 and 4) clearly demonstrates the inhibiting effect of lead on hydrogen evolution, particularly in the germanium-containing electrolyte where the presence of lead causes the cathodic current density to remain low. The Pb^{2+} ions adsorb or deposit at the active sites on zinc and/or germanium and they block the hydrogen evolution on the whole electrode. Moreover, the corrosion potential of zinc in lead-containing electrolyte is always more noble than that without additive. This confirms that zinc corrosion was also hindered by adsorbed lead on zinc, even in the presence of Ge^{4+} ions.

In the case of the aluminium cathode, both polarization curves obtained in the base electrolyte with and without germanium were much more polarized than those on the zinc electrode. The current density obtained from the germanium-containing electrolyte (lower than $0.5\,mA\,cm^{-2}$ in the potential domain from -1.4 to $-1.6\,V$) was about two times higher than that from germanium-free electrolyte. Consequently, in comparison with hydrogen evolution taking place on zinc deposits and germanium sites, hydrogen evolution on bare aluminium sites can be disregarded in our results.

The current density of curve 2 in Fig. 1, which is under zinc deposition conditions, is larger than that of curve 2 in Fig. 3. However, the difference in current densities between them is not entirely used for zinc deposition. This difference probably originates from physical properties, such as hydrogen evolution sites, morphology and orientation of commercial zinc metal, which are not the same as those of zinc deposits, and also from changes in the surface area due to the deposit dissolution in the presence of germanium.

As not only hydrogen evolution but also zinc dissolution occurs at cathodic potentials near the corrosion potential [15], it is of interest to take account of the effect of germanium on the dissolution of a pure zinc metal electrode. Figure 4 shows the steady-state polarization curves obtained by changing the potential from $-1.4\,V$ up to $-1.5\,V$, with the base electrolyte without additive (curve 1), with germanium (curve 2), with lead (curve 3) and with both germanium and lead (curve 4), respectively.

At anodic potentials, it is found that the slope of curves 2 and 4 is steeper and zinc dissolution is less polarized in comparison with curves 1 and 3. This means that germanium also activates zinc dissolution and probably increases the surface area of the zinc electrode. The activation of both hydrogen evolution and zinc dissolution causes the slope of curves 2 and 4 to become steeper at cathodic potentials.

Curves 2 and 4 show a minimum value at about $-1.47\,V$. Although in this study the electrolyte was

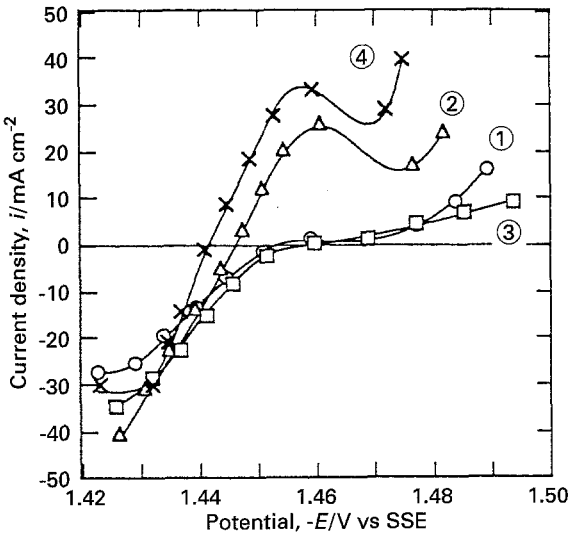

Fig. 4. Steady state polarization curves i/E obtained on zinc electrode from $U = -1.4\,V$ up to $-1.5\,V$ vs SSE in the base electrolyte. Curve 1: without additive; curve 2: with $0.5\,mg\,dm^{-3}$ germanium; curve 3: with $10\,mg\,dm^{-3}$ lead; curve 4: with both additives.

prepared using high purity reagents, it still contained a few impurities as mentioned. These impurities, especially trace lead, affected the surface reaction in terms of a competition between the effect of germanium and that of lead. The slow adsorption of lead on the zinc metal electrode probably induces the decrease in the cathodic current of hydrogen evolution observed at $-1.46\,V$ on curves 2 and 4. The inhibiting effect of lead on hydrogen evolution also explains the polarized region which can be seen near the corrosion potential on curves 1 and 3 obtained with germanium-free electrolytes. This behaviour disappears at high cathodic potential where zinc deposition occurs.

Comparing curves 1 and 3 also shows that Pb^{2+} ions in the electrolyte do not inhibit the dissolution of the zinc electrode which has been directly polarized at anodic potentials. This agrees with an

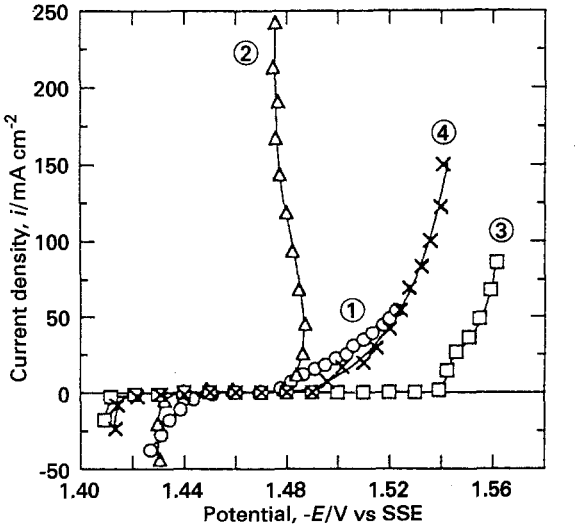

Fig. 5. Steady state polarization curves i/E obtained from $U = -1.4\,V$ up to $-1.6\,V$ vs SSE on predeposited zinc electrodes. Curve 1: without additive; curve 2: with $0.5\,mg\,dm^{-3}$ germanium; curve 3: with $10\,mg\,dm^{-3}$ lead; curve 4: with both additives.

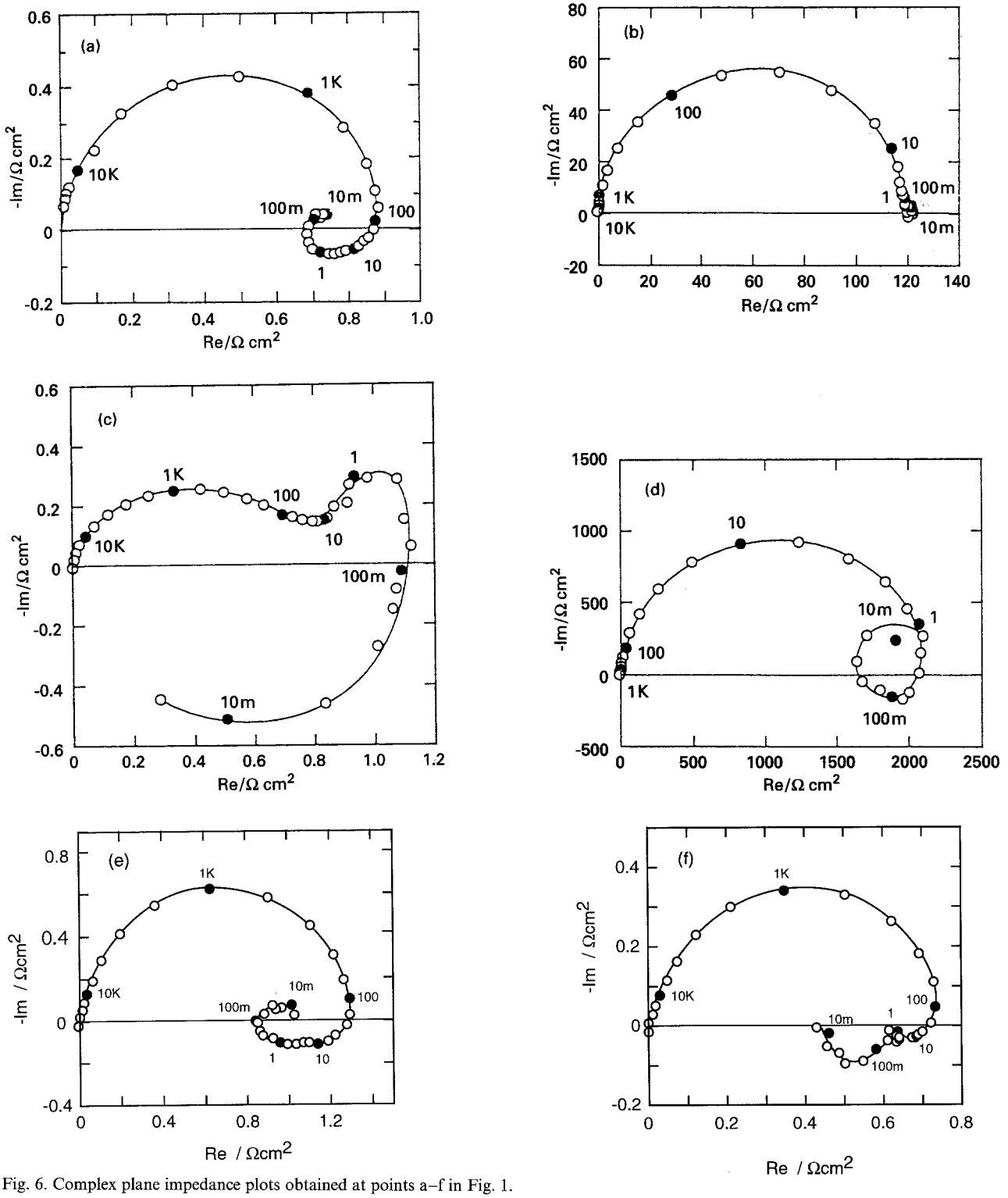

Fig. 6. Complex plane impedance plots obtained at points a–f in Fig. 1.

inhibition process governed by the slow adsorption and accumulation of lead at the electrode surface, impossible to realize on a permanently dissolving metal, but possible to achieve when the cathodic polarization was slowly stepped down, as in the cases of Figs 1 and 3, where lead could accumulate on the electrode near the corrosion potential.

Figure 5 shows the effect of additives on the dissolution of zinc predeposited on the aluminium substrate for 2 h, at a potential, U, of -1.56 V. For curves 1 and 2, zinc was pre-deposited in the base electrolyte without additive. For curve 3, it was prepared with lead, and for curve 4, with germanium and lead. Then, starting from $U = -1.4$ V up to -1.6 V, the current was measured after stabilization. Curve 1 was obtained in the base electrolyte without additive, curve 2 with germanium, curve 3 with lead, and curve 4 with both germanium and lead, respectively.

At anodic potentials, the current density on curves 1 and 2 is much higher than on curves 3 and 4. All curves show a plateau region near the corrosion potential, due to the lead codeposited with zinc during preelectrodeposition. Remaining on the

electrode surface, lead inhibits zinc dissolution (curves 3 and 4) and also hydrogen evolution and zinc deposition on curve 3. Cathodically, lead progressively desorbs and allows the hydrogen evolution to develop considerably in the germanium-containing electrolyte (curve 2). Similarly to Fig. 1, the cathodic curves 1 and 4 are close to each other due to a quasi-compensation between the inhibition by lead and the activation by germanium when both elements are present.

3.2. *Impedance analysis*

The impedance plots characteristics of hydrogen evolution and zinc deposition in base electrolyte with and without additives are depicted in Fig. 6. The symbols (a)–(f) correspond to those on the polarization curves in Fig. 1. Figure 6(a) shows the general features for zinc deposition in acidic electrolyte at highly cathodic potential [11, 20] and it consists of three parts: a capacitive loop with a characteristic frequency of 1.5 kHz due to the charge transfer resistance of zinc deposition and the double layer capacitance, an inductive loop with a characteristic medium frequency of 2 Hz and a low-frequency capacitive loop, possibly due to the partial diffusion control of zinc deposition on stationary electrode [19]. Figure 6(b), obtained on the plateau region on curve 1 in Fig. 1, only shows a capacitive loop due to hydrogen evolution, as already reported [19].

The effect of germanium on cathodic reactions clearly appears in the impedance characteristics. All impedance spectra obtained at cathodic potential in the base electrolyte with germanium show the features of Fig. 6(c) which characterize the hydrogen evolution mechanism induced by the presence of adsorbed germanium on zinc. These plots consist of two capacitive loops with characteristic frequencies of 1 kHz, and 1 Hz at high and medium frequencies, respectively, and of a low-frequency inductive loop with a characteristic frequency of 10 mHz. The size of the medium frequency capacitive loop decreased with decreasing cathodic overpotential.

The features of Fig. 6(d) characterize the hydrogen evolution reaction on the aluminium substrate, after completion of the dissolution of zinc deposits. Similar impedance plots were obtained on the aluminium electrode during hydrogen evolution in sulfuric acid.

Figure 6(e) is typical of impedance plots on curve 3 obtained from the lead-containing electrolyte. The difference with Fig. 6(a), which is characteristic of zinc deposition, resides in two separate inductive loops with characteristic frequencies of 12 and 1 Hz, respectively, in the medium frequency domain. These two inductive loops suggest that the lead affects the multistep discharge mechanism of Zn^{2+} ions involving the intermediate Zn^{+}_{ad} and the inhibiting adsorbate H_{ad}. Our previous work [11] and that of Frazer [7] showed that the trace lead present in the electrolyte inhibited the deposition process, thus enhancing the inhibition by H_{ad}.

The characteristics of impedance plots on curve 4 are depicted in Fig. 6(f). In comparison with Fig. 6(e), it reveals a better separation of the two inductive loops, with characteristic frequencies of 10 and 0.1 Hz. It also appears that the capacitive loop characteristic of hydrogen evolution on germanium in Fig. 6(c) has been cancelled by the presence of lead.

Impedance diagrams obtained from sulfuric acid solution are shown in Fig. 7. Over the whole potential range and under the same conditions as for curve 1 in Fig. 3, the electrode impedance exhibits only one capacitive loop, Fig. 7(g), due to the hydrogen evolution on zinc, similarly to Fig. 6(b). Under the conditions of curve 2 in Fig. 3, two capacitive loops and a low frequency inductive loop are exhibited on Fig. 7(h), similarly to Fig. 6(c). Figures 6(c) and 7(h) characterize the kinetics of hydrogen evolution on the zinc electrode probably covered with adsorbed germanium.

The potential dependence of the electrode kinetics is also apparent in Fig. 8 and Fig. 9 which represent the variation of the product of the transfer resistance, R_t, and current density, i, as a function of the electrode potential, E. These figures have been obtained under the same conditions as Fig. 1 and Fig. 3, respectively. The increase in $R_t i$, observed on curves 1, 3 and 4 in Fig. 8 with increasing cathodic potential from −1.5 to −1.56 V, characterizes the zinc deposition process, as already shown [11, 19, 20]. On the other hand, each curve in Fig. 8 has a peak in the potential domain −1.44 to −1.48 V as a result of hydrogen evolution [7, 11, 20]. It is clear that the $R_t i$ peak on curve 3, obtained from the lead-containing electrolyte, is much higher than on any other curves, thus indicating a lessened activation of hydrogen evolution with polarization, due to the lead adsorbed on the zinc electrode. This peak only appears when lead accumulates on the electrode surface near the corrosion potential: it was not observed during the dissolution of a pure zinc electrode from −1.4 V up to −1.5 V, but it existed during the dissolution of a zinc deposit in the same potential domain.

A lessened activation of hydrogen evolution by lead is confirmed in sulfuric solution, Fig. 9: $R_t i$ increases from about 70 mV on curve 1 to about 160 mV on curves 3 and 4, even with the presence of germanium. It is noticeable that curves 1, 3 and 4 do not exhibit a real plateau in the cathodic domain, but a maximum. This maximum, more pronounced on curves 3 and 4, probably resulted from the slow accumulation of lead on the electrode surface when the cathodic polarization was stepped down from −1.6 V.

The values of the double layer capacitance C_{dl}, deduced from the apex of the high frequency loop on the impedance plots, are given in Fig. 10, the electrolyte and experimental conditions for curves 1 to 4 being the same as for Fig. 1. With decreasing cathodic potential from −1.56 V, the capacitances

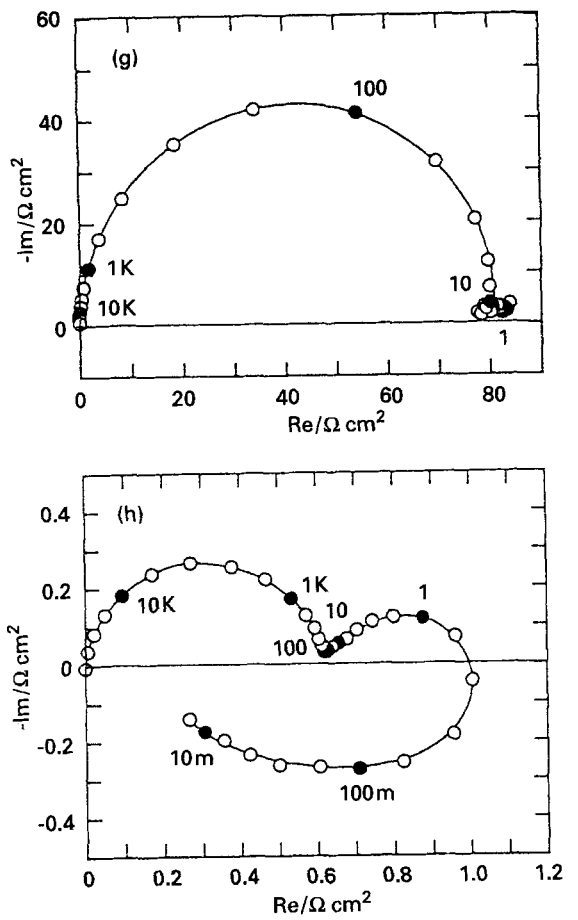

Fig. 7. Complex plane impedance plots obtained at points g and h in Fig. 3.

on curves 1, 3 and 4 decrease to about 25 μF cm^{-2}, as the deposition current progressively vanishes. This decreasing capacitance is connected with an increasing amount of adsorbed hydrogen and lead on the electrode: a value of 20 μF cm^{-2} characterizes the zinc electrode during hydrogen evolution in the H_2SO_4 solution, under the condition of curves 1, 3 and 4 in Fig. 3. The increase in C_{dl}, observed at

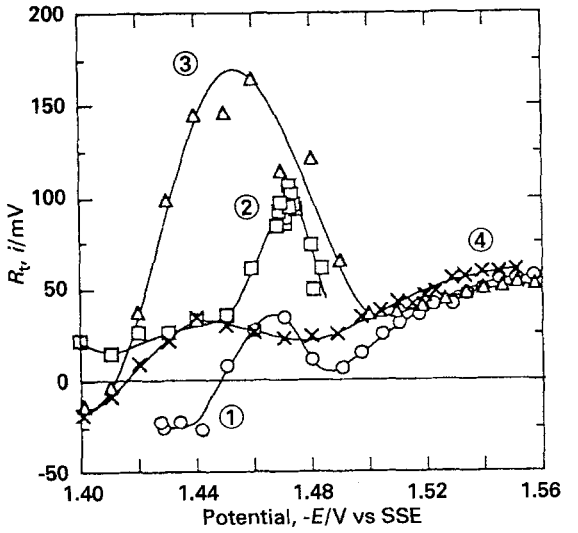

Fig. 8. Potential dependence of the product $R_t i$ obtained under the same conditions as in Fig. 1. Curve 1: without additive; curve 2: with 0.5 mg dm^{-3} germanium; curve 3: with 10 mg dm^{-3} lead; curve 4: with both additives.

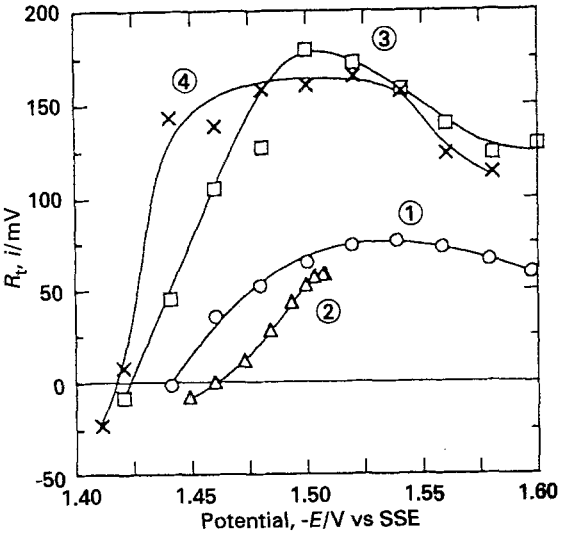

Fig. 9. Potential dependence of the product $R_t i$ for hydrogen evolution obtained under the same conditions as in Fig. 3. Curve 1: without additive; curve 2: with 0.5 mg dm^{-3} germanium; curve 3: with 10 mg dm^{-3} lead; curve 4: with both additives.

potentials close to −1.42 V on curve 1, is due to the dissolution of the zinc deposit in the base electrolyte.

Curve 2 in Fig. 10 also shows that with the germanium-containing electrolyte, the capacitance decreases from 400 to 10 μF cm^{-2}: this decrease is correlated with a decreasing effective surface area due to the total dissolution of the initially rough and ring-shaped deposit. The value of 10 μF cm^{-2} is typical of hydrogen evolution on the aluminium substrate.

4. Conclusion

From polarization curves, it has been verified that germanium adsorbed on the zinc electrode strongly stimulates hydrogen evolution on zinc deposits and causes their dissolution in acidic sulphate electrolytes.

Typical impedance plots have been obtained for zinc deposition or hydrogen evolution. Hydrogen evolution on zinc only reveals the charge transfer resistance and

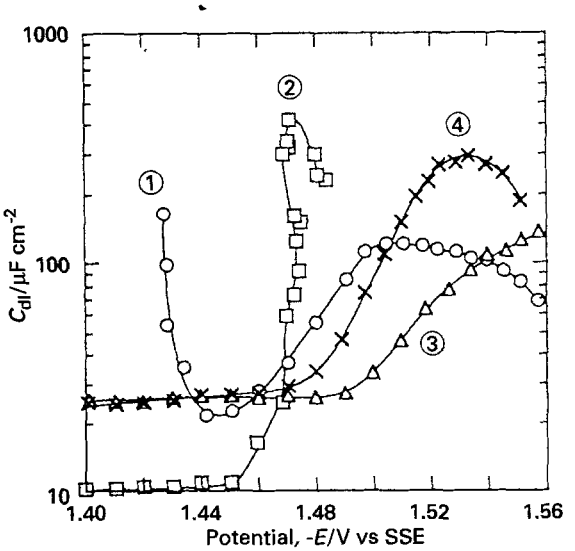

Fig. 10. Potential dependence of the double layer capacitance obtained under the same conditions as in Fig. 1.

the double layer capacitance. The kinetics of hydrogen evolution on germanium adsorbed on the electrode appears to be characterized by both a medium-frequency capacitive loop and a large inductive loop at low frequencies.

The inhibiting influence of lead, mainly on hydrogen evolution but also on zinc deposition and zinc dissolution, has been confirmed. Impedance plots reveal that the $R_t i$ product, associated with hydrogen evolution, increases markedly in the presence of lead. This indicates that the lead adsorbed on the zinc electrode results in a lessened activation for hydrogen evolution with increasing polarization. This inhibiting effect of lead only appears when lead can accumulate on the zinc electrode, for example, during hydrogen evolution in the sulfuric acid solution or during zinc deposition at small cathodic potentials. The influence of lead also results in a clear separation between the two inductive loops observed during zinc deposition, thus indicating that lead affects the kinetics of reactions involved in the multi-step mechanism for zinc deposition, particularly by enhancing the formation of H_{ad} on the zinc deposit.

With the addition of Pb^{2+} ions in the germanium-containing electrolyte, the formation of fine-grained zinc deposits is stabilized, and the features characteristic of zinc deposition prevail in the electrode impedance measurements.

The double layer capacitance is also a parameter which characterizes the electrode surface. On the one hand, it allows the change in the electrode surface area to be followed during the total dissolution of the rough deposits obtained from the germanium-containing electrolyte. On the other hand, during zinc deposition from the base electrolyte or from lead-containing electrolytes, its variation is evidence of the increasing deposit coverage by H_{ad} and adsorbed lead with decreasing cathodic polarization.

Acknowledgements

One of the authors (R. Ichino) wishes to acknowledge the Fellowship by the Ministry of Science, Education and Culture in Japan.

References

[1] M. Maja and P. Spinelli, *J. Electrochem. Soc.* **118** (1971) 1538.
[2] S. Oyama and K. Taniuchi, *J. Mining and Materials Processing Inst. Japan* **90** (1974) 781.
[3] D. R. Fosnacht and T. J. O'Keefe, *J. Appl. Electrochem.* **10** (1980) 495.
[4] M. Maja, N. Penazzi, R. Fratesi and G. Roventi, *J. Electrochem. Soc.* **129** (1982) 2695.
[5] Y. Umetsu and K. Tozawa, *J. Mining and Minerals Processing Inst. Japan* **102** (1986) 429.
[6] A. R. Ault and E. J. Frazer, *J. Appl. Electrochem.* **18** (1988) 583.
[7] E. J. Frazer, *J. Electrochem. Soc.* **135** (1988) 2465.
[8] C. Bozhkov, M. Petrova and S. T. Rashkov, *J. Appl. Electrochem.* **20** (1990) 17.
[9] D. J. Mackinnon, J. M. Brannen and P. L. Fenn, *ibid.* **17** (1987) 1129.
[10] R. Wiart, C. Cachet, Chr. Bozhkov and S. T. Rashkov, *ibid.* **20** (1990) 381.
[11] C. Cachet, R. Wiart, I. Ivanov and S. Rashkov, *ibid.* **23** (1993) 1011.
[12] D. J. Mackinnon, J. M. Brannen and R. C. Kerby, *ibid.* **9** (1979) 55.
[13] D. J. Mackinnon and J. M. Brannen, *J. Appl. Electrochem.* **7** (1977) 451.
[14] D. R. Fosnacht and T. J. O'Keefe, *Metall. Trans. B* **14B** (1983) 645.
[15] D. J. Mackinnon and P. L. Fenn, *J. Appl. Electrochem.* **14** (1984) 467.
[16] M. Sider and D. L. Piron, *J. Appl. Electrochem.* **18** (1988) 54.
[17] D. J. Mackinnon, R. M. Morrison, J. E. Mouland and P. E. Warren, *ibid.* **20** (1990) 728.
[18] C. Cachet, R. Wiart, I. Ivanov, Y. Stefanov and S. Rashkov, *ibid.* **24** (1994) 713.
[19] C. Cachet and R. Wiart, *ibid.* **20** (1990) 1009.
[20] *Idem, J. Electrochem. Soc.* **141** (1994) 131.
[21] F. Mansfeld and S. Gilman, *ibid.* **117** (1970) 588.
[22] S. Higuchi, S. Takahashi and Y. Miyake, *Denki Kagaku* **39** (1971) 522.
[23] J. Bressan and R. Wiart, *J. Appl. Electrochem.* **7** (1977) 505.
[24] H. Krug and Borchers, *Electrochim. Acta*, **13** (1968) 2203.